Energy Reports 7 (2021) 2113–2124

Contents lists available at ScienceDirect

Energy Reports

journal homepage: www.elsevier.com/locate/egyr

Research paper

An optimized algorithm for optimal power flow based on deep learning

Qinggang Su [a], Habib Ullah Khan [b], Imran Khan [c], Bong Jun Choi [d], Falin Wu [e,*], Ayman A. Aly [f]

[a] School of Intelligent Manufacturing and CDKIP, Shanghai Dianji University, Shanghai, 201306, China
[b] Department of Accounting and Information System, College of Business and Economics, Qatar University, Doha 2713, Qatar
[c] Department of Electrical Engineering, University of Engineering and Technology Peshawar, Pakistan
[d] School of Computer Science and Engineering, Soongsil University, South Korea
[e] School of Instrumentation and Optoelectronic Engineering, Beihang University, Beijing, 100191, China
[f] Department of Mechanical Engineering, College of Engineering, Taif University, P.O. Box 11099, Taif 21944, Saudi Arabia

ARTICLE INFO

Article history:
Received 15 February 2021
Received in revised form 30 March 2021
Accepted 12 April 2021
Available online 21 April 2021

Keywords:
Power systems
Deep learning
Transient stability
Power optimization
Sustainable energy

ABSTRACT

With the increasing requirements for power system transient stability assessment, the research on power system transient stability assessment theory and methods requires not only qualitative conclusions about system transient stability but also quantitative analysis of stability and even development trends. Judging from the research and development process of this direction at home and abroad in recent years, it is mainly based on the construction of quantitative index models to evaluate its transient stability and development trend. Regarding the construction theories and methods of quantitative index models, a lot of results have been achieved so far. The research ideas mainly focus on two categories: uncertainty analysis methods and deterministic analysis methods. Transient stability analysis is one of the important factors that need to be considered. Therefore, this paper proposed an optimized algorithm based on deep learning for preventive control of the transient stability in power systems. The proposed algorithm accurately fits the generator's power and transient stability index through a deep belief network (DBN) by unsupervised pre-training and fine-tuning. The non-linear differential–algebraic equation and complex transient stability are determined using the deep neural network. The proposed algorithm minimizes the control cost under the constraints of the contingency by realizing the data-driven acquisition of the optimal preventive control. It also provides an efficient solution to stability and reliability rules with similar safety into the corresponding control model. Simulation results show that the proposed algorithm effectively improved the accuracy and reduces the complexity as compared with existing algorithms.

1. Introduction

The power system is a strategic system for national economic development, and its stable operation guarantees the energy supply needed for economic development. With the development of my country's economic level, the level of electricity consumption is increasing, the scale of the system is increasing, the network structure is more complex, the operating point of the system is getting closer to the stability limit, and the requirements for the prevention and control of power system stability are getting higher and higher. Transient instability is often the main cause of large-scale power system accidents. Effective power system transient stability assessment and accident prevention measures are the key to solving this problem (Narciso and Martins, 2020; Mocanu et al., 2019; Alsafasfeh et al., 2020; Martin et al., 2019; Kang et al., 2020).

Traditional transient stability calculations usually use time-domain simulation plus appropriate criteria, which have the advantages of accurate calculation and high reliability. However, the model contains nonlinear differential–algebraic equations, which are complicated and takes a long time to calculate, which is difficult to meet the requirements of online calculation (Liu et al., 2020, 2019; Alsafasfeh et al., 2019c,b). Artificial intelligence algorithms can establish the mapping relationship between data input and output through learning, and the calculation speed is fast, so it is used for transient stability assessment and avoid complex time-domain equation solving (Alsafasfeh et al., 2019a; Shakerighadi et al., 2020; Kang et al., 2017; Bhui and Senroy, 2017; Shiwei et al., 2019; Yousefian et al., 2017; Li et al., 2018a;

* Corresponding author.
E-mail addresses: qinggangsu@sina.com (Q. Su), habib.khan@qu.edu.qa (H.U. Khan), imran_khan@uetpeshawar.edu.pk (I. Khan), davidchoi@soongsil.ac.kr (B.J. Choi), falin.wu@buaa.edu.cn (F. Wu), Aymanaly@tu.edu.sa (A.A. Aly).

https://doi.org/10.1016/j.egyr.2021.04.022

Shetye et al., 2016). Literature (Hu et al., 2019) uses data preprocessing algorithms such as feature variable selection, cluster analysis, and maximum entropy discrete method to reduce the data dimension and then applies the association classification method for temporary stability evaluation. Literature (Au et al., 2019) proposed a temporary stability evaluation method based on the synthesis of multiple support vector machines (SVM), which integrated multiple sets of high-accuracy SVM evaluation results to reduce the rate of misjudgment.

In the literature (Hu et al., 2019; Au et al., 2019), although methods such as data preprocessing and joint judgment of multiple good models are used to improve accuracy, they are all based on human feature extraction. The models have incomplete feature extraction and feature extraction errors, resulting in low evaluation accuracy. Literature (Hou et al., 2018a) uses a combination model of probabilistic neural network and radial basis network for transient stability evaluation and critical removal time estimation. However, its neural network model has a small number of network layers, and its ability to mine and learn the inherent laws of the data is limited, and it has the problems of low accuracy and poor convergence. Literature (Zhang et al., 2018) uses stacked autoencoders to achieve the two functions of feature extraction and transient stability evaluation while using sparse technology and Dropout technology to improve generalization capabilities. Compared with machine learning and neural network methods, the deep learning model has the advantages of automatic feature extraction, strong abstraction ability, and good convergence. Its network structure is deeper and it is more conducive to discovering the internal laws of data. However, the literature (Zhang et al., 2018) only proposed a transient stability evaluation method and did not combine the deep learning method with the generator active output control strategy to solve the transient instability control problem of the power system. Preventive control refers to the identification of the current system state before the system fails, the potential failure risk of the system is discovered in advance, and the system is adjusted to a state where the system can still operate stably after the failure by adjusting the generator output and changing the load size (Mahdi and Genc, 2018). Combining preventive control with transient stability, a transient stability preventive control (TSPC) is proposed to ensure that the system runs in a state that meets the requirements of transient stability (Yan et al., 2015). Literature (Xie et al., 2020) uses trajectory sensitivity to analyze the corresponding relationship between the trajectory changes of generator power angle and active power output and system stability to improve the transient stability of the system, but the process requires multiple time-domain simulation calculations and calculation time It is difficult to meet the requirements of online applications. Literature (Yousefian et al., 2017) uses a neural network model combined with short-term memory to determine the transient stability of the system. The neural network model and stability margin are used in the preventive control sensitivity model to realize preventive control. Literature (Wawrzyniak et al., 2020) adds a neural network model based on literature (Shiwei et al., 2019) to increase the speed of generating preventive control strategies. Literature (Passaro et al., 2014) combined BP network and genetic algorithm to generate transient stability evaluation model, and embedded it in particle swarm algorithm to evaluate the transient stability of preventive control strategy. The BP network used in the literature (Passaro et al., 2014) has only 3 layers, which is difficult to fit complex nonlinear equations. Although it is combined with a genetic algorithm to improve the accuracy of model evaluation, it is necessary to repeatedly try different initial training points and model structures, which reduces the speed of model training. Literature (Darbandi et al., 2020) uses two-stage SVM for transient stability assessment, but only uses linear equations obtained by linear SVM for preventive control. The transient stability boundary of the system is simply equivalent to a high-dimensional plane. The model is relatively simple and difficult to guarantee The accuracy of system preventive control and optimal strategy.

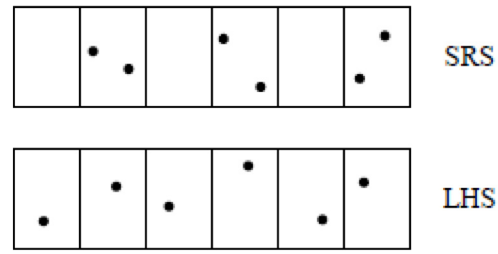

Fig. 1. Illustrations of Latin Hypercube Sampling and simple random sampling.

Aiming at the above problems, a deep learning-driven power system transient stability preventive control evolutionary algorithm is proposed. First, establish a set of power system transient stability estimators based on a deep confidence network, and its network structure. Compared with the traditional neural network, the structure has a deeper scale. It can learn the deeper internal laws of the measurement data and the stability margin under the condition of unmanned feature extraction to fit the mapping relationship between generator output and transient stability and has the convergence advantages of strong ability and good generalization. After the training of the transient stability, the estimator is completed, it is different from traditional machine learning methods which are usually used for state mapping and matching identification. In this paper, the trained transient stability evaluator is embedded as a non-explicit “box-constraints” for evolution. In the iterative optimization process of the algorithm, the expected failure was realized under the set constraint, the data-driven retrieval technology of power generation rescheduling prevention control optimization strategy to minimize the control cost can also provide a method reference for similar security, stability, and reliability rules embedded in the corresponding control strategy model and efficient solution.

2. Transient stability evaluation based on deep belief network

2.1. Optimal power flow model with transient stability constraints

Traditional power system transient stability calculations use the transient stability constraint optimal power flow (TSCOPF) model (Li et al., 2020; Wu et al., 2021; Guangchao et al., 2017), which adds transient stability constraints based on the optimal power flow model. The purpose of the model is to solve the optimal operating point of the system when all the constraints of the power system are met so that the objective function reaches the optimal value. The mathematical expression of TSCOPF is as follows.

2.1.1. Objective function

The objective function of TSCOPF is to minimize the total cost of power generation which is expressed as

$$\min f(x) = \sum_{i \in S_g} \left(a_{G_i} P_{G_i}^2 + b_{G_i} P_{G_i} + c_{G_i} \right) \quad (1)$$

where $f(x)$ is the total cost of power generation; S_g is the generator set; P_{G_i} contributes power to the generator; a_{G_i}, b_{G_i}, and c_{G_i} are cost factors.

Table 1
Samples of DL model.

Sample		Label value
n is the number of generators k is the number of samples l is the number of preset failures	$\begin{cases} P_{G1}^{1}, \ldots, P_{Gn}^{1} \\ \vdots \\ P_{G1}^{k}, \ldots, P_{Gn}^{k} \end{cases}$	$\begin{cases} \min\left(\mathrm{TSI}_1^1, \ldots, \mathrm{TSI}_l^1\right) \\ \vdots \\ \min\left(\mathrm{TSI}_1^k, \ldots, \mathrm{TSI}_l^k\right) \end{cases}$

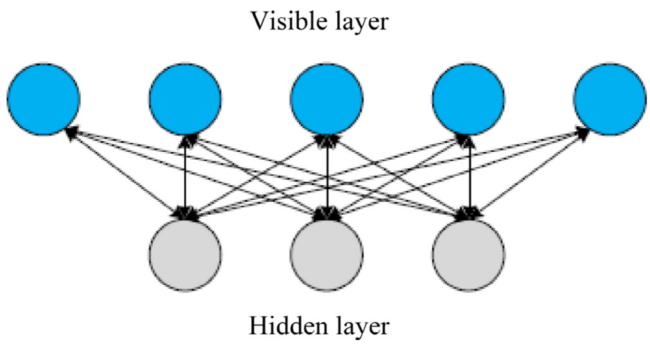

Fig. 2. Restricted Boltzmann machine structure.

2.1.2. Equality constraints

The node filling power balance equation is expressed as

$$\begin{cases} P_{Ni} = P_{Di} - V_i \sum_{j=1}^{n} V_j \left(G_{ij}^0 \cos\alpha_{ij} + B_{ij}^0 \sin\alpha_{ij}\right) \\ Q_{Ni} = Q_{Di} - V_i \sum_{j=1}^{n} V_j \left(G_{ij}^0 \sin\alpha_{ij} - B_{ij}^0 \cos\alpha_{ij}\right) \end{cases} \quad i = S_n \tag{2}$$

where P_{Ni} and Q_{Ni} are node active and reactive filling power; P_{Di} and Q_{Di} are node active and reactive output power; V_i and V_j are the node voltage amplitudes; α_{ij} is the phase angle difference of node voltage; Gij and Bij are the real and imaginary parts of the node admittance; S_n is the set of nodes.

2.1.3. Inequality constraints

The stable operation constraints are expressed as

$$\begin{cases} P_{Gi}^{\min} \le P_{Gi} \le P_{Gi}^{\max}, & i \in S_g \\ Q_{Gi}^{\min} \le Q_{Gi} \le Q_{Gi}^{\max}, & i \in S_g \\ V_i^{\min} \le V_i \le V_i^{\max}, & i \in S_n \\ P_{ij}^{\min} \le P_{ij} \le P_{ij}^{\max}, & (i,j) \in S_1 \end{cases} \tag{3}$$

where $P_{Gi}^{\max}$ and $P_{Gi}^{\min}$ are the upper and lower limits of the generator's active power output; $Q_{Gi}^{\max}$ and $Q_{Gi}^{\min}$ are the upper and lower limits of reactive power output; $V_i^{\max}$ and $V_i^{\min}$ are the upper and lower limits of node voltage; $P_{ij}^{\max}$ and $P_{ij}^{\min}$ are the upper and lower limits of the line thermal stability constraints; S_1 is the line set.

2.1.4. Transient stability constraints

The expressions for transient stability constraints are expressed as:

$$\frac{dx}{dt} = f(x, y, \lambda) \tag{4}$$

$$h(x, y, \lambda) = 0 \tag{5}$$

where x is the state variable; y is the algebraic variable; λ is the control variable. Eq. (4) is a differential equation whereas Eq. (5) is an algebraic equation.

Eqs. (4) and (5) include the solution of nonlinear differential–algebraic equations in the calculation process, the calculation complexity is high, the calculation time is long, and there are many fault sets in the large power grid, which doubles the difficulty of calculation, and it is difficult to meet the transient

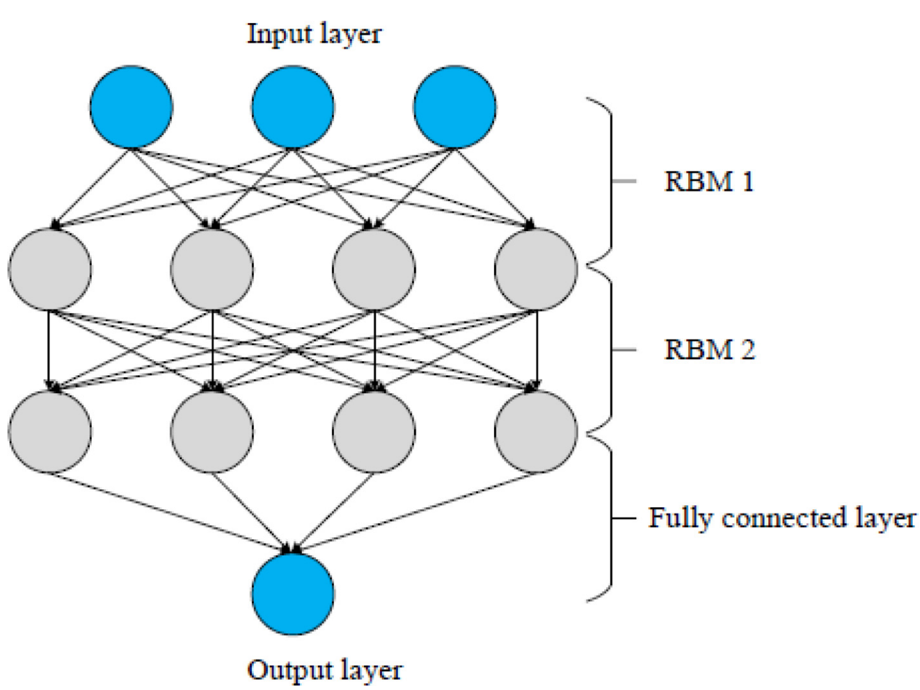

Fig. 3. Structure of deep belief network.

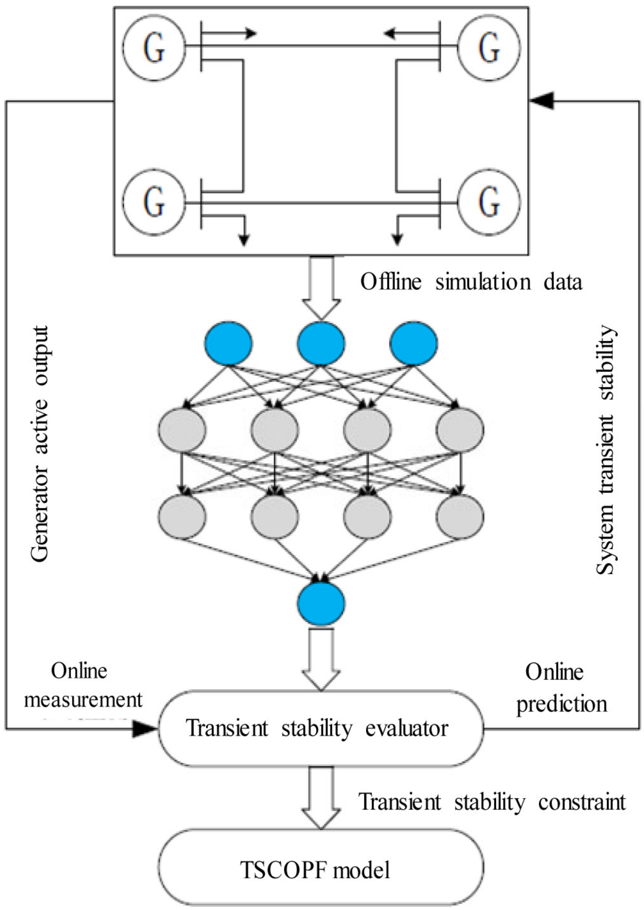

Fig. 4. Deep belief network-based transient stability analysis.

Table 2
Expected failure set.

Fault number	System fault line		
	39 node system	68-node system	140-node system
1	2-3	1-2	16-17
2	3-4	1-30	17-18
3	3-18	2-3	2-33
4	4-5	2-25	2-3
5	4-14	3-4	3-4
6	5-6	3-18	5-31
7	16-17	4-5	9-30
8	16-21	42-51	7-15
9	16-24	48-40	29-30
10	17-27	4-14	32-35

Table 3
Comparison of accuracy.

Test system	Accuracy of transient stability estimator (%)
10-machine 39-node system	98.3
16 machine 68 node system	97.8
48 machine 140 node system	97.5

stability online, Therefore, the transient stability estimator based on DBN is proposed for calculation requirements.

2.2. Sample generation

2.2.1. Transient stability coefficient

Select TSI as the transient stability evaluation index. TSI reflects the maximum power angle difference of the generator during the transient state. The Transient Security Assessment Tool (TSAT) based on angle margin algorithm that calculates the TSI (Jovica, 2016; Gautam et al., 2009; Cipriano et al., 2018; Sajadi et al., 2017). The mathematical expression of TSI is:

$$\mathrm{TSI} = \frac{360 - \delta_{\max}}{360 + \delta_{\max}} \times 100 \tag{6}$$

where $\delta_{\max}$ is the maximum power angle difference between any two generators in the system. When TSI > 0, the system is transiently stable, and the larger the TSI value, the higher the system transient stability; when TSI < 0, the system is transiently unstable.

2.2.2. Latin hypercube sampling and predicted failure set

Latin Hypercube Sampling (LHS) is used to generate a sample space where the generator's active power output fluctuates within a certain range, and according to the principle of active power balance and load power factor constant, the load active and reactive power fluctuates with the generator's active power. LHS divides the sample value range into N equal parts according to the number of samples N, and randomly selects a point in each equal part, so that the sample spreads over the entire sample space and has a certain degree of randomness. Fig. 1 shows the comparison between LHS and simple random sampling (SRS) (Shiwei et al., 2016).

It can be seen from Fig. 1 that LHS is more evenly distributed than SRS samples, and the sample data generated by LHS is more conducive to improving the generalization ability of the transient stability estimator.

Select several lines as the expected fault set, and select one of them as the fault line in each time-domain simulation calculation. At the same time, the fault type is selected as a three-phase short-circuit fault to ensure that the deep learning model can evaluate the TSI corresponding to the most serious fault in all fault situations.

2.2.3. Transient stability calculation and inertial center transformation

Combine all generator output samples and expected fault lines in sequence, as the initial conditions of time-domain simulation, use the power system toolbox (PST) for time-domain simulation calculation, record the generator power angle changes, and calculate TSI (Li et al., 2018b; Youness et al., 2019; Yagami et al., 2020; Ray, 2017; Mylonas et al., 2020; Sabo et al., 2020).

When recording the power angle curve, take the center of inertia (COI) as the reference line to perform COI transformation on the rotor angle δ_i of each generator. The mathematical expression is:

$$\delta_{\mathrm{COI}} = \delta_i - \delta_0 \tag{7}$$

$$\delta_0 = \frac{1}{M_{\mathrm{T}}} \sum_{i \in S_g} M_i \delta_i \tag{8}$$

$$M_{\mathrm{T}} = \sum_{i \in S_g} M_i \tag{9}$$

where δ_{COI} is the generator power angle after COI conversion; δ_0 is COI; M_i is the generator inertia constant (Minye and Lingling, 2016; Cheema and Mehmood, 2020; Mujcinagic et al., 2020; Dakovic et al., 2020; Tabora and Smith, 1972).

2.2.4. Deep learning model samples

In the case of the same generator output, it is expected that each fault in the fault cluster corresponds to one TSI. To ensure the transient stability requirements for any fault line and fault type, the smallest TSI value is selected as the effective output of this generator. The corresponding TSI constitutes the sample data for training the transient stability estimator.

The sample data is shown in Table 1.

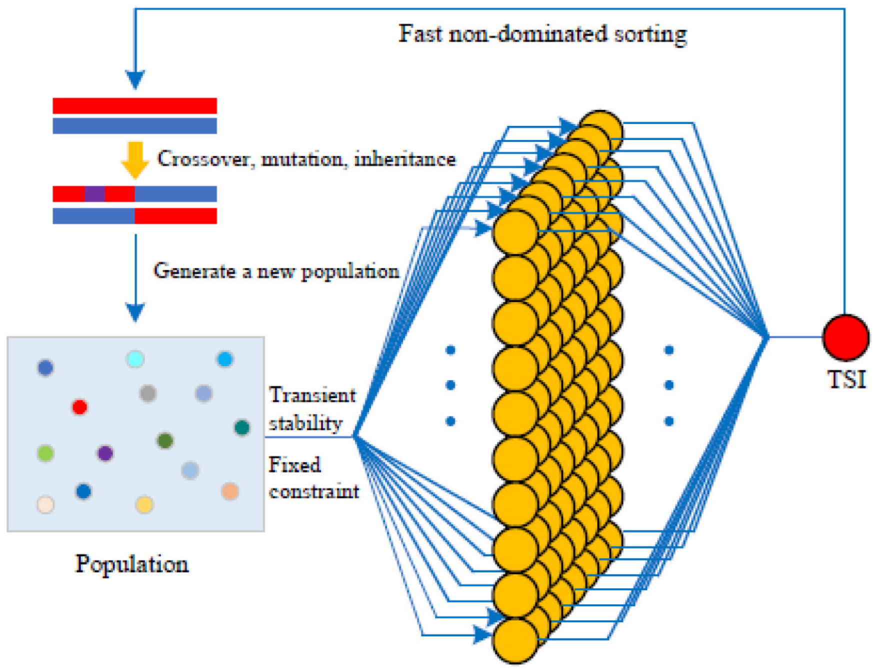

Fig. 5. Proposed DL algorithm process.

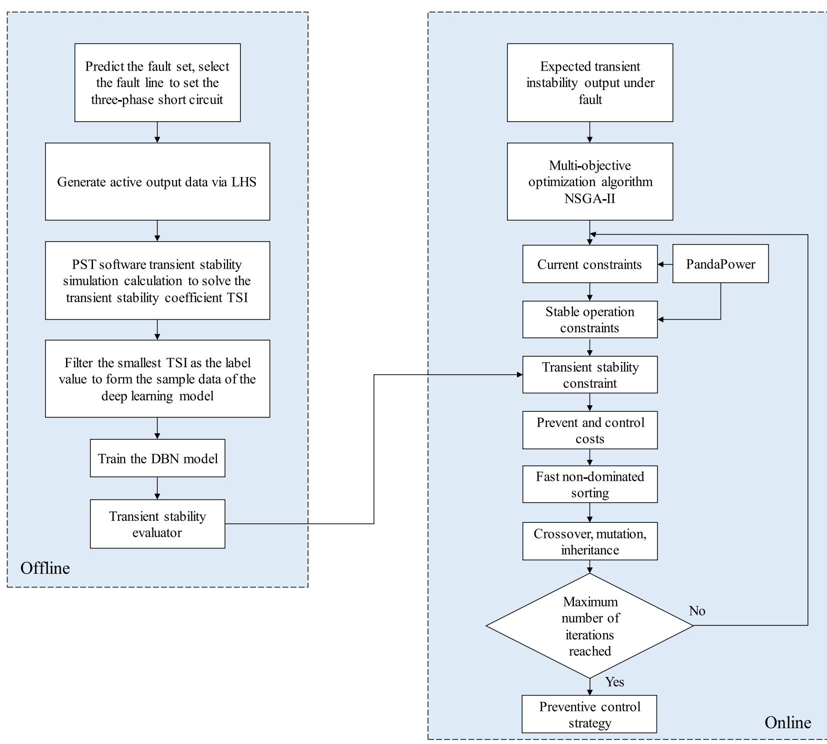

Fig. 6. Proposed algorithm flowchart.

2.3. Deep belief network

DBN is composed of a multi-layer restricted Boltzmann machine (RBM) and a fully-connected layer, which has the advantages of automatic feature extraction, strong nonlinear representation, robustness, etc. Compared with the neural network model, it has a deeper model structure and better abstraction ability, which can extract more complex internal laws of the power system. Therefore, DBN is used to evaluate the transient stability of the power system.

2.3.1. Restricted Boltzmann machine

RBM is a randomly generated neural network, including 1 visible layer and 1 hidden layer. Neurons in the same layer are independent of each other, while neurons in different layers are bidirectionally connected. When training RBM, information flows in two directions, and the weights in the two directions are the same, and the biases are different. The RBM structure is shown in Fig. 2.

RBM is a probability distribution model based on energy. The model consists of an energy function and a probability distribution function based on the energy function. For a given state vector ($\boldsymbol{h}$, $\boldsymbol{v}$), the energy function of RBM is

$$E(\boldsymbol{v}, \boldsymbol{h}) = -\boldsymbol{a}^{\mathrm{T}}\boldsymbol{v} - \boldsymbol{b}^{\mathrm{T}}\boldsymbol{h} - \boldsymbol{h}^{\mathrm{T}}\boldsymbol{W}\boldsymbol{v} \tag{10}$$

where $\boldsymbol{v}$ is the visible layer unit matrix; $\boldsymbol{h}$ is the hidden layer unit matrix; $\boldsymbol{a}$ is the bias matrix of the visible layer unit; $\boldsymbol{b}$ is the bias matrix of the hidden layer unit set matrix; $\boldsymbol{W}$ is the connection weight matrix between the visible layer unit $\boldsymbol{v}$ and the hidden layer unit $\boldsymbol{h}$.

The joint probability distribution function of $\boldsymbol{v}$ and $\boldsymbol{h}$ in RBM is

$$P(\boldsymbol{v}, \boldsymbol{h}) = \frac{1}{Z} e^{-E(\boldsymbol{v}, \boldsymbol{h})} \tag{11}$$

where $Z = \sum_{\boldsymbol{v},\boldsymbol{h}} e^{-E(\boldsymbol{v},\boldsymbol{h})}$ is called the normalization constant of the partition function.

Since the partition function is difficult to handle, the maximum likelihood gradient approximation is used to derive the conditional distribution from the joint distribution:

$$P(h_j = 1|v) = \mathrm{sigmoid}\left(w_{:,j} v_j + b_j\right) \tag{12}$$

$$P(v_j = 1|h) = \mathrm{sigmoid}\left(w_{:,j} h_j + a_j\right) \tag{13}$$

where $\mathrm{sigmoid} = 1/\left(1 + e^{-x}\right)$ is the activation function.

The training objective of RBM is to minimize the loss function, which is

$$L(W, a, b) = -\sum_{i=1}^{m} \ln\left(P\left(v^{(i)}\right)\right) \tag{14}$$

2.3.2. Deep belief network

DBN has composed of multiple layers of RBM and a layer of the fully connected layer. Its structure is shown in Fig. 3. DBN model training is divided into two stages. The first stage is pre-training. Each layer of RBM uses unlabeled sample data for greedy layer-by-layer unsupervised learning. Through pre-training, the DBN model is near the optimal solution, which solves the problem that deep neural networks cannot be trained due to gradient loss or gradient explosion. The second stage is to use labeled sample data to train the model as a whole, through stochastic gradient descent. Algorithm and backpropagation make the weights and biases fine-tuned based on pre-training to achieve the best fitting effect (Lan et al., 2007).

The energy function and joint probability function of DBN are:

$$E\left(v, h^1, h^2, h^3\right) = -v^{\mathrm{T}} W^1 h^1 - h^{1\mathrm{T}} W^2 h^2 - h^{2\mathrm{T}} W^3 h^3 \tag{15}$$

$$P\left(v, h^1, h^2, h^3\right) = \frac{1}{Z} e^{-E\left(v, h^1, h^2, h^3\right)} \tag{16}$$

The learning rate decay method, mean square error (MSE), and L2 regularization are used in the model training process. The method of learning rate attenuation can improve the learning speed in the early stage of training, and improve the evaluation accuracy rate in the later stage of training; the gradient of MSE loss decreases as the loss decreases. When the loss approaches 0, the gradient is very small. At the end of the training, the MSE is more absolute than the mean absolute error (MAE) calculation results are more accurate; L2 regularization can prevent the model from overfitting. The mathematical expressions are:

$$L_r = L_r \times \frac{1}{1 + D \times E} \tag{17}$$

$$MSE = \frac{1}{m} \sum_{i=1}^{m} \left(\Phi(x_i) - y_i\right)^2 \tag{18}$$

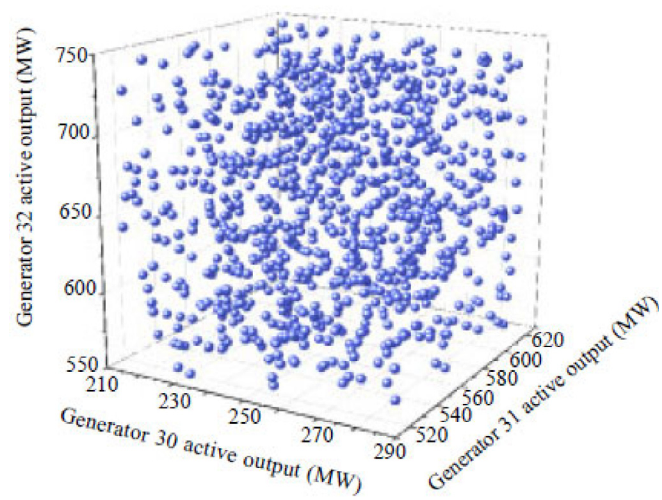

Fig. 7. Comparison of output power through LHS.

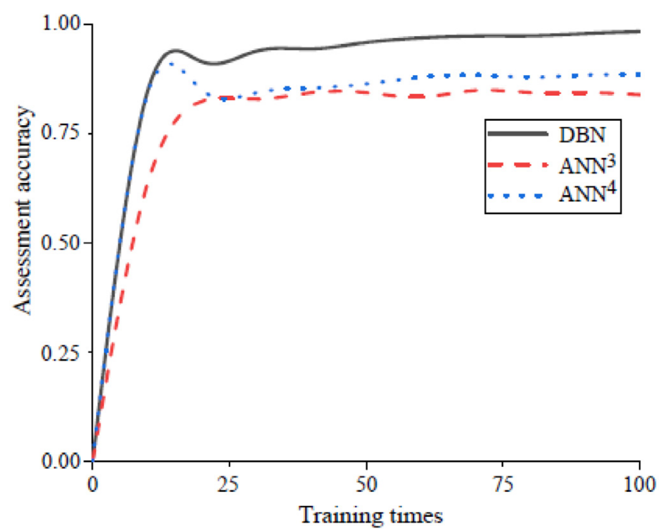

Fig. 8. Accuracy comparison of the proposed and existing algorithms.

$$f(x) = \min\left[\frac{1}{m}\sum_{i=1}^{m}\left(\Phi(x_i) - y_i\right)^2 + \lambda \sum_{j=1}^{n} \omega_j^{\,2}\right] \tag{19}$$

where L_r is the learning rate; D is the learning rate attenuation coefficient; E is the number of training; $\Phi(x)$ is the DBN model; x_i is the training set; y_i is the tag value corresponding to x_i; m is the number of training set samples; n is the number of DBN layers; ω_i is the weight coefficient; λ is the regularization parameter.

2.4. DBN model training

The active power output of the generator in the sample data is used as the DBN input vector, and TSI is used as the corresponding label value to learn the nonlinear mapping relationship between the two. After training, the transient stability constraint represented by the DBN model can be expressed as

$$\Phi\left(P_{G1}^{\mathrm{pre}}, P_{G2}^{\mathrm{pre}}, \ldots, P_{Gn}^{\mathrm{pre}}\right) > 0 \tag{20}$$

where P_G^{pre} is the active power output of the generator given by the preventive control; $\Phi(P_G)$ is the trained DBN model. Its input is the active power output of all generators in the system, and the output is the TSI evaluated by the model. When the

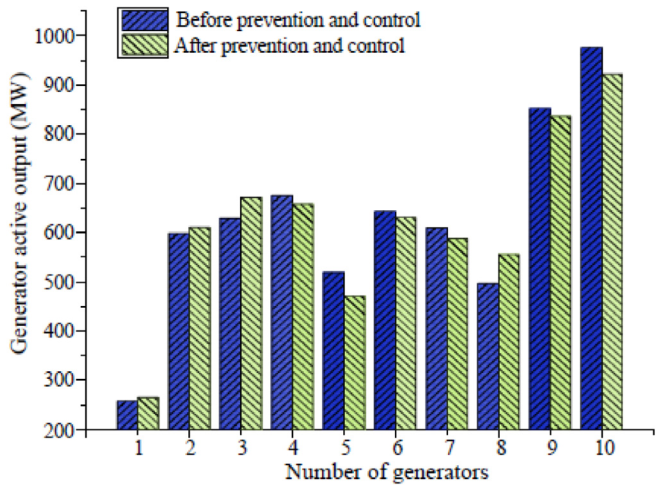

Fig. 9. Generator power comparison with and without the proposed algorithm.

evaluated TSI > 0, the DBN model considers the system transient state under this active output. On the contrary, it is considered that the system is transiently unstable, and preventive control is required. The training process of the DBN-based power system transient stability estimator is shown in Fig. 4.

3. DBN-driven transient stability preventive control

3.1. NSGA-II algorithm optimization goal

NSGA-II is developed from the NSGA algorithm and has the advantages of low computational complexity, high population diversity, fast running speed, and good solution set convergence (Hou et al., 2018b). NSGA-II is a multi-objective optimization algorithm that can find optimization results that satisfy multiple constraints at the same time. In this paper, NSGA-II has 4 optimization objectives, namely: preventive control and adjustment cost, power flow constraint, stable operation constraint, and transient stability constraint (Nezamabad et al., 2019). The NSGA-II algorithm will consider the calculation results of 4 optimization targets at the same time and give the optimal preventive control strategy. The cost function of the NSGA-II algorithm is:

$$\min F_{\text{cost}} = \sum_{i \in S_g} \left(C_{\text{U}i} \left| \Delta P_{\text{U}i} \right| + C_{\text{D}i} \left| \Delta P_{\text{D}i} \right| \right) \tag{21}$$

$$\Delta P_{\text{U}i} = \begin{cases} P_{pi} - P_{\text{O}i}, & P_{pi} > P_{\text{O}i} \\ 0, & P_{pi} \le P_{\text{O}i} \end{cases} \tag{22}$$

$$\Delta P_{\text{D}i} = \begin{cases} 0, & P_{pi} \ge P_{\text{O}i} \\ P_{pi} - P_{\text{O}i}, & P_{pi} < P_{\text{O}i} \end{cases} \tag{23}$$

where $C_{\text{U}i}$ increases the cost of generator output; $C_{\text{D}i}$ reduces the cost of generator output; $P_{\text{O}i}$ is used to prevent and control the generator output; P_{pi} is the generator's output after preventive control; $\Delta P_{\text{U}i}$ is the increased value of generator output; $\Delta P_{\text{D}i}$ is the reduced value of generator output.

3.2. DBN-NSGA-II preventive control algorithm

Embed PandaPower and DBN-based transient stability estimator in the NSGA-II algorithm to form the DBN-NSGA-II preventive control algorithm. Use PandaPower to judge the current constraints and stable operation constraints of the population, and the transient stability estimator to evaluate the individual TSI. In the case of DBN with high accuracy, the output of the DBN model can be regarded as the TSI in the case of this active work. The way the transient stability estimator is embedded in NSGA-II is shown in Fig. 5.

The calculation process of the DBN-NSGA-II algorithm is shown in Fig. 6.

3.3. Usability improvement

In each iteration of the NSGA-II algorithm, all population individuals are substituted into the objective function, the corresponding results are calculated, and fast non-dominated sorting is performed according to the size of the results. The computational complexity of the NSGA-II algorithm is

$$\mathcal{O}\left(mN^2\right) \sim \mathcal{O}\left(mN^3\right) \tag{24}$$

where m is the number of objective functions; N is the population size, the population increases, and the computational complexity increases from 2 to 3 times.

In this model, the transient stability of the system is the primary indicator and must be above a certain stability threshold. Therefore, after the transient stability estimator obtains the individual TSI value, individuals whose TSI value is less than a certain stability threshold are eliminated. In the subsequent iteration process, due to the rapid reduction of the population size, the NSGA-II algorithm can quickly complete the iteration. At the same time, considering the conservativeness of prevention and control, the critically unstable samples are marked as needing control intervention, and 50 is selected as the threshold for screening population individuals. At this time, the accuracy of transient stability assessment can reach 100%.

4. Case analysis

4.1. Sample set construction

A 10-machine 39-node system, a 16-machine 68-node system, and a 48-machine 140-node system were selected to verify the performance of the algorithm. Select 10 lines of all lines in each system as the expected fault lines, and set the three-phase to short-circuit faults in the middle of the lines to form the expected fault set. The expected failure set is shown in Table 2.

Because of the expected fault concentrated fault lines and fault types, the active power output of the generator is set to fluctuate in the range of 90% to 110%. Using Latin hypercube sampling to generate 1000 kinds of generator active output, and according to the principle of active power balance and load power factor constant, the system load active and reactive power will fluctuate as the total generator active output changes. Combine these 1000 types of generator active power output conditions with 10 expected fault lines concentrated with expected failures to form 10,000 types of expected failure data. Use PST to perform time-domain simulation calculation on the expected fault data, set the fault removal time to 0.1s, and the total simulation time to 20 s to solve the corresponding TSI. Each generator output corresponds to 10 TSIs, the smallest TSI among the 10 TSIs is screened, and the generator output together forms 1000 sample data for training the transient stability estimator. Fig. 7 shows the Latin hypercube sampling results of generators 30, 31, and 32 in the 39-node system.

It can be seen from Fig. 7 that the data in the sample space formed by generators 30, 31, and 32 are evenly distributed throughout the entire sample space, which is beneficial to improve the generalization ability of the transient stability estimator.

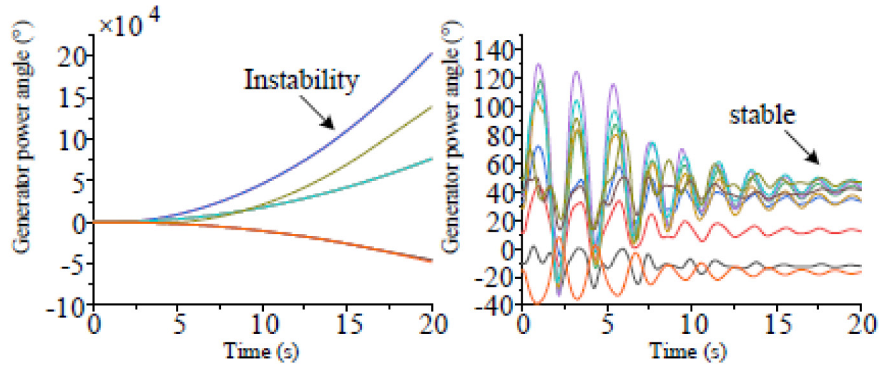

(a) Fault 7 preventive control before (left) and after (right)

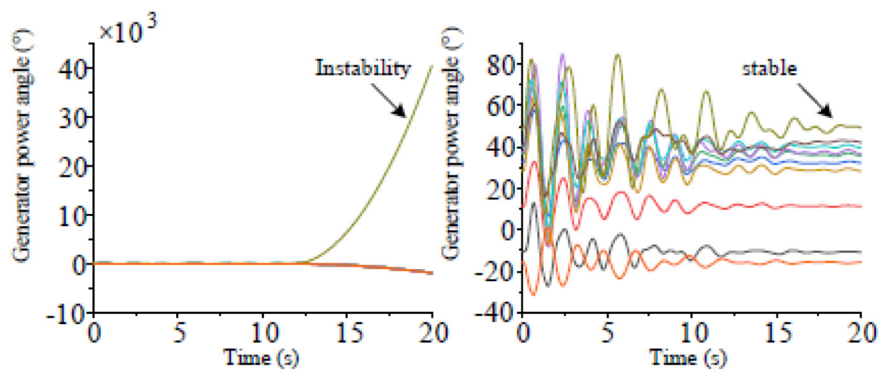

(b) Fault 10 before (left) and after (right) preventive control

Fig. 10. Angular comparison of the power with and without the proposed algorithm for 7 and 10 faults.

Table 4
Cost comparison.

Power generation Machine	Before prevention and control Power output (MW)	After prevention and control Power output (MW)	Active effort adjustment Section size (MW)	Unit tone Cost-saving	Single machine Cost-saving	Total adjustment Cost
1	258.6	265.6	6.9	10	69.0	
2	599.0	610.8	11.7	10	117.0	
3	629.7	672.0	42.4	10	424.0	
4	675.6	658.1	−17.5	5	87.5	
5	519.5	471.9	−47.6	5	238.0	
6	642.8	630.8	−11.9	5	59.5	1805
7	610.3	588.1	−22.1	5	110.5	
8	496.7	556.2	59.5	10	595.0	
9	852.5	836.4	−16.1	5	80.5	
10	976.8	922.0	−4.8	5	24.0	

Table 5
Comparison of the TSI with and without control for the proposed and reference Jovica (2016).

Fault number	Before and after control											
	39 node system				68 node system				140 node system			
	Before		After		Before		After		Before		After	
	Ref. Jovica (2016)	Proposed	Ref. Jovica (2016)	Proposed	Ref. Jovica (2016)	Proposed	Ref. Jovica (2016)	Proposed	Ref. Jovica (2016)	Proposed	Ref. Jovica (2016)	Proposed
1	66.8	68.7	68.3	69.5	70.1	71.8	74.1	75.2	−98.4	−97.0	69.5	70.3
2	67.1	68.9	68.7	69.4	69.9	71.6	73.8	74.8	−97.2	−96.1	65.3	66.2
3	67.2	68.9	68.4	69.3	70.8	72.6	74.4	75.5	66.5	67.2	69.6	70.5
4	67.6	69.5	69.5	70.2	70.9	72.7	74.5	75.6	65.3	66.4	68.5	69.2
5	67.9	68.8	68.8	69.4	70.2	71.9	73.8	74.8	65.3	66.4	68.5	69.2
6	68.1	69.0	68.9	69.5	70.3	72.0	73.9	74.9	67.3	68.1	68.8	69.7
7	−107.4	−99.7	69.3	69.9	70.3	72.0	74	75.0	66.9	67.6	68.9	70.0
8	67.9	68.6	69.2	69.6	−61.5	−57.9	59.8	61.6	67.2	67.9	68.8	69.7
9	68.5	69.3	69.5	70.0	−82.7	−76.2	58.4	60.6	66.1	67.0	68.7	69.4
10	−104.5	−98.3	68.7	69.5	70.3	72.0	74	75.0	67.1	68.0	68.8	69.7

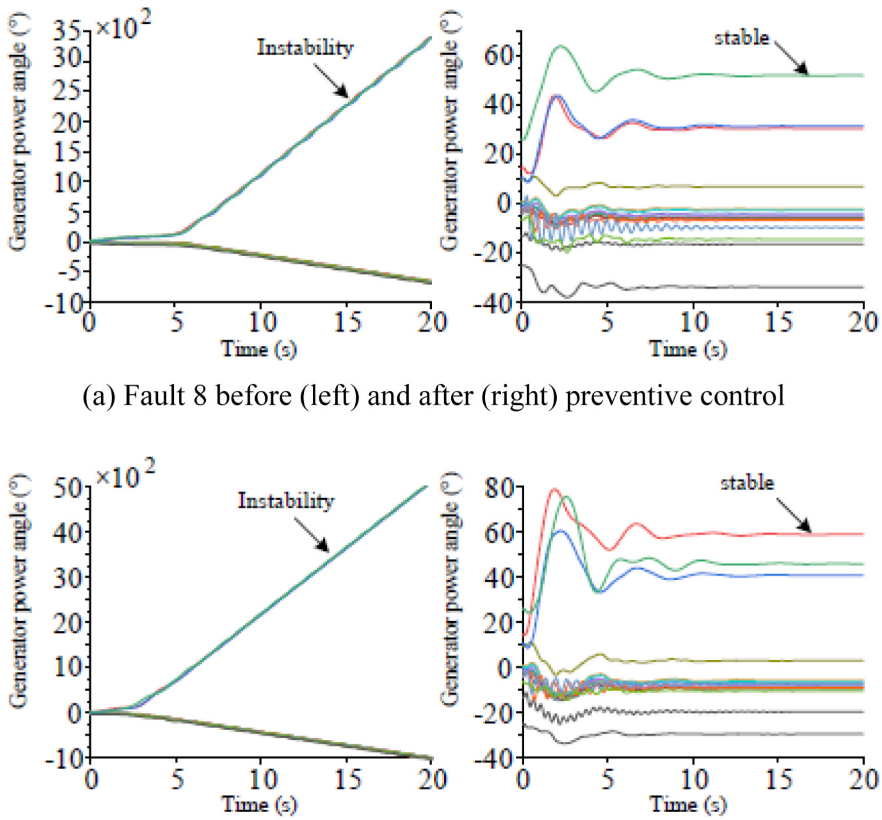

(a) Fault 8 before (left) and after (right) preventive control

(b) Fault 9 preventive control before (left) and after (right)

Fig. 11. Angular comparison of the power with and without the proposed algorithm for 8 and 9 faults.

Table 6
Applicability improvement comparison.

Test System	Population Size	Algorithm	TSI	Cost control USD	Calculation Time (s)	Amount of power not delivered to the system (MW)	Cost of wasted power (USD)
10-machine 39-node system	2000	DBN-NSGA-II	87.2	1921	4840.00	6.3	213
		Improved DBN-NSGA-II	86.3	1805	13.90	3.2	103
	1000	DBN-NSGA-II	52.5	1999	957.00	4.7	176
		Improved DBN-NSGA-II	71.5	2053	4.03	2.5	93
	500	DBN-NSGA-II	88.4	1960	201.00	3.9	123
		Improved DBN-NSGA-II	62.1	2240	1.90	2.1	84
16 machine 68 node system	2000	DBN-NSGA-II	59.6	9032	4952.00	7.2	274
		Improved DBN-NSGA-II	63.9	11287	35.70	4.5	145
	1000	DBN-NSGA-II	60.0	8011	1028.00	6.8	242
		Improved DBN-NSGA-II	63.3	10931	7.88	3.9	123
	500	DBN-NSGA-II	59.8	9180	223.00	6.2	204
		Improved DBN-NSGA-II	63.5	11955	2.41	3.3	95
48 machine 140 node system	2000	DBN-NSGA-II	64.3	10931	5443.00	7.8	289
		Improved DBN-NSGA-II	64.1	10643	36.30	4.7	151
	1000	DBN-NSGA-II	64.6	10959	999.00	7.2	274
		Improved DBN-NSGA-II	64.8	13532	8.70	3.7	103
	500	DBN-NSGA-II	64.8	10690	209.00	6.1	218
		Improved DBN-NSGA-II	63.5	12672	2.43	2.8	94

4.2. Performance evaluation of transient stability estimator

Divide the 1000 sample data into a training set containing 800 data and a test set containing 200 data, use the training set to train the transient stability estimator, and verify the accuracy of the model through the test set. The recognition accuracy of different test systems is shown in Table 3.

Construct two artificial neural networks (ANN) models. The first ANN has 3 layers, the number of neurons is 10, 100, and 1, denoted as ANN3, and the second is 4 layers. It adopts the same network structure as DBN and The number of neurons, the number of neurons is 10, 100, 50, 1 in order, and it is recorded as ANN4. Taking the 10-machine 39-node system as the test system, under the same conditions of calculation tools, optimizer,

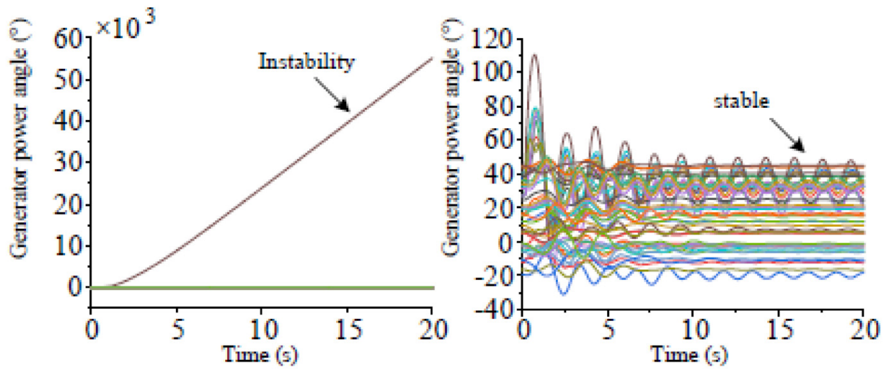

(a) Fault 1 before (left) and after (right) preventive control

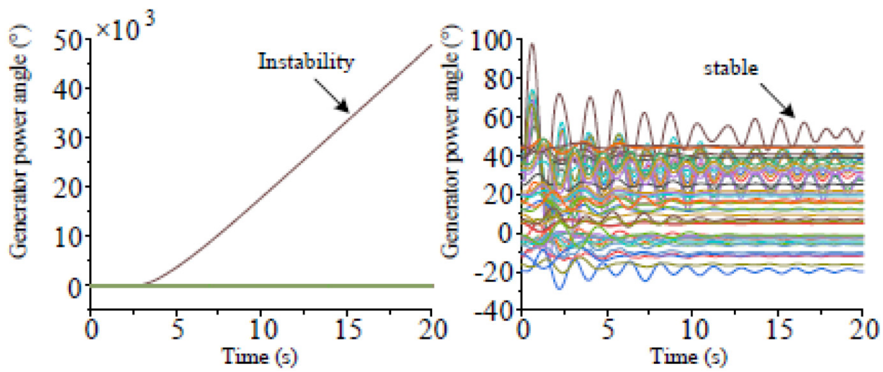

(b) Fault 2 before (left) and after (right) preventive control

Fig. 12. Angular comparison of the power with and without the proposed algorithm for faults 1 and 2.

activation function, and loss function, the accuracy of the three models under different iteration times is counted, and the result is shown in Fig. 8.

It can be seen from Fig. 8 that DBN has the fastest convergence speed and the best evaluation results compared with the other two ANNs. The result in Fig. 8 shows the role of the DBN model pre-training. Through pre-training, the DBN model reaches the vicinity of the optimal solution. After the overall model training, the best fitting effect can be quickly obtained.

4.3. Analysis of the results

The DBN-based transient stability evaluator is embedded in the NSGA-II algorithm to perform transient stability preventive control on the output of transient unstable generators. The output comparison before and after the prevention control of the 39-node system is shown in Fig. 9, and the adjustment cost of the prevention control is shown in Table 4.

Finally, PST is used to verify the preventive control strategy, and the time-domain simulation method is used to calculate the TSI before and after the preventive control under each expected failure. The comparison of the TSI before and after the preventive control of each test system is shown in Table 5. It can be seen from Table 5 that the transient instability faults before preventive control become transiently stable after preventive control. The transiently stable faults before preventive control remain transiently stable, and the TSI has increased slightly, indicating that the strategy has been appropriately increased. Temporary stability margin of the system for full fault set.

Fig. 10 shows the power angle curve before and after the preventive control of the 39-bus system under fault 7 and fault 10.

Fig. 11 shows the power angle curve before and after the preventive control of the 68-bus system under fault 8 and fault 9.

Fig. 12 shows the power angle curve before and after the preventive control of the 140-node system under fault 1 and fault 2.

From the comparison of power angle curves before and after preventive control in Figs. 10–12, it can be seen that through predictive control, the system returns from transient instability to transient stability.

4.4. Applicability improvement result analysis

Considering the conservativeness of prevention and control, the critically unstable samples are marked as needing control intervention, and 50 is selected as the threshold for screening population individuals. At this time, the assessment accuracy of the transient stability evaluator can reach 100%. Therefore, to improve the DBN-NSGA-II algorithm, in the iterative process, the stability threshold is selected as 50, that is, the TSI > 50 prevention control strategy is considered to be transiently stable, and the corresponding individual is retained in the offspring, while TSI < 50 individuals are eliminated, through a certain cost increase, to ensure the reliability of preventive control strategies. The calculation time of TSI, adjustment cost, and prevention control strategy before and after the applicability improvement is compared for different test systems in different population sizes, as shown in Table 6. It can be seen from the results in Table 6 that using the improved DBN-NSGA-II algorithm while keeping the TSI and cost within a good range, the computing time can be greatly improved, and better preventive control can be obtained within a few seconds. Strategies to meet the requirements of online prevention and control.

5. Conclusion

Different from traditional machine learning algorithms, which are mostly used for state identification and evaluation, this paper proposes a power system transient stability prevention control evolutionary algorithm embedded in a deep confidence network, using the combination of NSGA-II algorithm intelligent optimization and deep confidence network accurate identification to achieve The rapid and stable search for the optimal strategy of transient stability prevention and control for the expected failure set is presented. Through the analysis of numerical examples, the following conclusions are obtained:

(1) The DBN-based transient stability estimator can accurately fit the mapping relationship between generator output and TSI, and greatly increase the speed of transient stability evaluation to meet online evaluation requirements.

(2) The DBN-driven power system transient stability preventive control evolutionary algorithm embeds the transient stability evaluator as a non-explicit "black box constraint" in the iterative optimization process of evolutionary calculation, and realizes the expected failure set the constraint to control the cost The data-driven search technology of the minimum-targeted power generation rescheduling preventive control optimization strategy meets the requirements of online preventive control.

The deep learning-driven evolutionary algorithm for transient stability prevention and control proposed in this paper combines deep learning and evolutionary algorithms to provide a new tool for online decision-making for transient stability prevention and control, and can also embed similar safety, stability, and reliability rules. Provide method reference in corresponding control strategy model.

In the next stage of research, we will consider the oscillation mode, transient energy, and various kinds of standby constraints, as a whole, take into account the proposed calculation framework, and continue to conduct applicability testing and improvement.

Funding

Taif University Researchers Supporting Project number (TURSP-2020/77), Taif university, Taif, Saudi Arabia.

CRediT authorship contribution statement

Qinggang Su: Writing, Revision, Final approval. **Habib Ullah Khan:** Writing, Revision, Final approval. **Imran Khan:** Writing, Revision, Final approval. **Bong Jun Choi:** Writing, Revision, Final approval. **Falin Wu:** Writing, Revision, Final approval. **Ayman A. Aly:** Writing, Revision, Final approval.

Declaration of competing interest

The authors declare that they have no known competing financial interests or personal relationships that could have appeared to influence the work reported in this paper.

Data availability

The data used for the findings of this study is available upon request from the corresponding authors.

Acknowledgment

This research was supported under the National Research Foundation (NRF), Korea (2019R1C1C1007277) funded by the Ministry of Science and ICT (MSIT), Korea.

References

Alsafasfeh, Q., Saraereh, O.A., Alsafasfeh, M., Maqableh, A., et al., 2020. An efficient algorithm for power flow optimization in PV inverters systems. Electr. Power Compon. Syst. 48 (12), 1362–1377.
Alsafasfeh, Q., Saraereh, O.A., Khan, I., Choi, B.J., 2019a. A robust decentralized power flow optimization for dynamic PV system. IEEE Access 7, 63789–63800.
Alsafasfeh, Q., Saraereh, O.A., Khan, I., Kim, S., 2019b. LS-solar-PV system impact on line protection. Electronics 8 (2), 1–13.
Alsafasfeh, Q., Saraereh, O.A., Khan, I., Kim, S., 2019c. Solar PV grid power flow analysis. Sustainability 11 (6), 1–17.
Au, N.N., Nghia, L.T., Anh, Q.H., Binh, P.T.T., 2019. Advanced parallel classifier model for dynamic stability diagnosis in power system. Ain Shams Eng. J. 10 (1), 45–53.
Bhui, P., Senroy, N., 2017. Real-time prediction and control of transient stability using transient energy function. IEEE Trans. Power Syst. 32 (2), 923–934.
Cheema, K.M., Mehmood, K., 2020. Improved virtual synchronous generator control to analyze and enhance the transient stability of microgrid. IET Renew. Power Gener. 14 (4), 495–505.
Cipriano, D., Rengifo, J., Aller, J.M., 2018. Transient stability evaluation of high penetration of DFIG controlled by DTC and DPC into power systems. In: IEEE Third Ecuador Technical Chapters Meeting. ETCM, Cuenca, Ecuador, pp. 1–6.
Dakovic, J., Krpan, M., Ilak, P., Barkrad, T., Kuzle, I., 2020. Impact of wind capacity share, allocation of inertia and grid configuration on transient rocof: the case of a croatian power system. Int. J. Electr. Power Energy Syst. 121, 1–8.
Darbandi, F., Jafari, A., Karimipouri, H., Dehghantanha, A., Derakhshan, F., et al., 2020. Real-time stability assessment in smart cyber-physical grids: a deep learning approach. IET Smart Grid 3 (4), 454–461.
Gautam, D., Vittal, V., Harbour, T., 2009. Impact of increased penetration of DFIG-based wind turbine generator on transient and small signal stability of power systems. IEEE Trans. Power Syst. 24 (3), 1426–1434.
Guangchao, G., Quanyan, J., Youxian, S., 2017. Parallel transient stability-constrained optimal power flow using GPU as coprocessor. IEEE Trans. Smart Grid 8 (3), 1436–1445.
Hou, K., Shao, G., Wang, H., Zhang, L., Zhang, Q., et al., 2018a. Research on practical power system stability analysis algorithm based on modified SVM. Prot. Control Mod. Power Syst. 11, 1–7.
Hou, J., Xie, C., Wang, T., Yu, Z., Lu, Y., et al., 2018b. Power system transient stability assessment based on voltage phasor and convolution neural network. In: IEEE International Conference on Energy Internet. ICEI, Beijing, China, pp. 1–6.
Hu, W., Lu, Z., Wu, S., Zhang, W., Dong, Y., et al., 2019. Real-time transient stability assessment in power system based on improved SVM. J. Modern Power Syst. Clean Energy 7, 26–37.
Jovica, M., 2016. Probabilistic stability analysis: the way forward for stability analysis of sustainable power systems. Phil. Trans. R. Soc. A 375, 1–22.
Kang, T., Lim, D.Y., Tayara, H., Chong, K.T., 2020. Forecasting of power demands using deep learning. Appl. Sci. 10 (20), 1–11.
Kang, T., Yao, J., Duong, T., Yang, S., Zhu, X., 2017. A hybrid approach for power system security enhancement via optimal installation of flexible AC transmission (FACTS) devices. Energies 10 (9), 1–21.
Lan, Z., Gan, D., Shi, L., Ni, Y., 2007. A study on the control of AC/DC power systems based on system dynamic COI. In: IEEE power engineering society meeting, Tampa, USA, pp. 1–7.
Li, N., Li, B., Gao, L., 2020. Transient stability assessment of power system based on XGBoost and factorization machine. IEEE Access 8, 28403–28414.
Li, B., Xaio, J., Wang, X., 2018a. Feature reduction for power system transient stability assessment based on neighborhood rough set and discernibility matrix. Energies 11 (1), 1–23.
Li, N., Zhu, Z., Li, M., Lin, Y., Wang, X., et al., 2018b. Research on reliability evaluation of power system including improved Monte Carlo and parallel calculation. In: IEEE International Conference on Power and Renewable Energy. ICPRE, Chengdu, pp. 1–7.
Liu, Z.F., Li, L.L., Tseng, M.L., Tan, R.R., Aviso, K.B., 2019. Improving the reliability of photovoltaic and wind power storage systems using least squares support vector machine optimized by improved chicken swarm algorithm. Appl. Sci. 9 (18), 1–16.
Liu, J., Sun, H., Li, Y., Fang, W., Niu, S., 2020. An improved power system transient stability prediction model based on mRMR feature selection and WTA ensemble learning. Appl. Sci. 10 (7), 1–20.
Mahdi, M., Genc, V.M.I., 2018. Post-fault prediction of transient instabilities using stacked sparse autoencoder. Electr. Power Syst. Res. 164, 243–252.
Martin, E.G., Rodrigues, C.F., Riley, G., Grahn, H., 2019. Estimation of energy consumption in machine learning. J. Parallel Distrib. Comput. 134, 75–88.
Minye, M., Lingling, F., 2016. Implementing consensus based distributed control in power system toolbox. In: IEEE North American Power Symposium, Denver, 2016, pp. 1–6.
Mocanu, E., Mocanu, D.C., Nguyen, P.H., Liotta, A., Webber, M.E., et al., 2019. On-line building energy optimization using deep reinforcement learning. IEEE Trans. Smart Grid 10 (4), 3698–3708.

Mujcinagic, A., Kuslugic, M., Nukic, E., 2020. Wind inertial response based on the center of inertia frequency of a control area. Energies 13 (23), 1–17.
Mylonas, E., Tzanis, N., Birbas, M., Birbas, A., 2020. An automatic design framework for real-time power system simulators supporting smart grid applications. Electronics 9 (2), 1–24.
Narciso, D.A.C., Martins, F.G., 2020. Application of machine learning tools for energy efficiency in industry: A review. Energy Rep. 6, 1181–1199.
Nezamabad, H.A., Zand, M., Alisadeh, A., Vosoogh, M., Nojavan, S., 2019. Multi-objective optimization based robust scheduling of electric vehicles aggregator. Sustainable Cities Soc. 47, 1–18.
Passaro, M.C., Silva, A.P., Lima, A.S., 2014. Preventive control stability via neural network sensitivity. IEEE Trans. Power Syst. 29 (6), 2846–2853.
Ray, P., 2017. Power system low frequency oscillation mode estimation using wide area measurement systems. Eng. Sci. Technol. Int. J. 20 (2), 598–615.
Sabo, A., Wahab, N.I., Othman, M.L., Jaffar, M.Z., Acikgoz, H., et al., 2020. Application of neuro-fuzzy controller to replace SMIB and interconnected multi-machine power system stabilizers. Sustainability 12 (22), 1–26.
Sajadi, A., Preece, R., Milanovic, J., 2017. Evaluation of suitability of different transient stability indices for identification of critical system states. In: 10^{th} Bulk Power Systems Dynamics and Control Symposium. IREP 2017, Brazil, pp. 1–6.
Shakerighadi, B., Peyghami, S., Ebrahimzadeh, E., Blaabjerg, F., Back, C.L., 2020. A new guideline for security assessment of power systems with a high penetration of wind turbines. Appl. Sci. 10 (9), 1–20.
Shetye, K.S., Overbye, T.J., Mohapatra, S., Gronquist, J.F., Doern, T.L., 2016. Systematic determination of discrepancies across transient stability software. IEEE Trans. Power Syst. 31 (1), 432–441.
Shiwei, X., Siqi, B., Junjie, H., et al., 2019. Efficient transient stability analysis of electrical power system based on a spatially paralleled hybrid approach. IEEE Trans. Ind. Inf. 15 (3), 1460–1473.
Shiwei, X., Xiao, L., Chan, K.W., et al., 2016. Probabilistic transient stability constrained optimal power flow for power systems with multiple correlated uncertain wind generations. IEEE Trans. Sustain. Energy 7 (3), 1133–1144.
Tabora, C.J., Smith, O.J.M., 1972. Characterization of equilibrium and stability in power systems. IEEE Trans. Power Appar. Syst. PAS-91 (3), 1127–1130.
Wawrzyniak, K., Padron, E.U., Jaworski, W., Korab, R., 2020. Risk-based active power redispatch optimization. Energies 13 (3), 1–20.
Wu, H., Shen, D., Xia, B., Qiu, Y., Zhou, Y., et al., 2021. Parametric problems in power system analysis: Recent applications of polynomial approximation based on Galerkin method. J. Mod. Power Syst. Clean Energy 9 (1), 1–12.
Xie, X., Xu, Y., Dong, Z.Y., Zhang, Y., Liu, J., 2020. Multi-objective coordinated dispatch of high wind-penetrated power systems against transient instability. IET Gener. Transm. Distrib. 14 (19), 4079–4088.
Yagami, M., Ichinohe, M., Tamura, J., 2020. Enhancement of power system transient stability by active and reactive power control of variable speed wind generators. Appl. Sci. 10 (24), 1–18.
Yan, X., Zhaoyang, D., Junhua, Z., et al., 2015. Trajectory sensitivity analysis on the equivalent one-machine-infinite-bus of multi-machine systems for preventive transient stability control. IET Gener. Transm. Distrib. 9 (3), 276–286.
Youness, E.M., Aziz, D., Abdelaziz, E.G., Jamal, B., Najib, E.O., et al., 2019. Implementation and validation of backstepping control of PMSG wind turbine using dSPACE controller board. Energy Rep. 5, 807–821.
Yousefian, R., Battarai, R., Kamalsadan, S., 2017. Transient stability enhancement of power grid with integrated wide area control of wind farms and synchronous generators. IEEE Trans. Power Syst. 32 (6), 4818–4831.
Zhang, R., Wu, J., Shao, M., Li, B., Lu, Y., 2018. Transient stability prediction of power systems based on deep belief networks. In: IEEE 2^{nd} International Conference on Energy Internet and Energy System Integration. EI2, Beijing, China, pp. 1–8.